Physica A 544 (2020) 124109

Contents lists available at ScienceDirect

Physica A

journal homepage: www.elsevier.com/locate/physa

Heat and mass transfer investigation of MHD Eyring–Powell flow in a stretching channel with chemical reactions

S. Hadi Seyedi [a,*], Behzad Nemati Saray [b], Ali J. Chamkha [c,d]

[a] Department of Mechanical Engineering, Wayne State University, 5050 Anthony Wayne Drive, Detroit, MI 48202, USA
[b] Department of Mathematics, Institute for Advanced Studies in Basic Sciences (IASBS), Zanjan 45137-66731, Iran
[c] Mechanical Engineering Department, Prince Mohammad Endowment for Nanoscience and Technology, Prince Mohammad Bin Fahd University, Al-Khobar 31952, Saudi Arabia
[d] RAK Research and Innovation Center, American University of Ras Al Khaimah, P.O. Box 10021, Ras Al Khaimah, United Arab Emirates

ARTICLE INFO

Article history:
Received 11 May 2019
Received in revised form 8 December 2019
Available online 7 January 2020

Keywords:
Eyring–Powell model
Magnetohydrodynamic (MHD)
Multi-wavelet Galerkin method
Stretching channel

ABSTRACT

In this paper, we studied the unsteady heat and mass transfer of magneto-hydrodynamics (MHD) Eyring–Powell squeezing flow in a channel by considering, radiation, chemical reaction and heat generation/absorption effects. Similarity solution was utilized to convert the 2-D governing partial differential equations to a set of non-linear ordinary differential equations and then a high accuracy spectral method based on the classical Galerkin approach developed to solve the equations. Comparison of the results with the fourth order Runge–Kutta method shows the accuracy and high agreement of the results for the velocity, temperature and concentration distribution in different locations of the channel. Effects of change in the values of several parameters on the velocity, temperature and concentration profiles were investigated. The results of the computation show that increasing the squeezing number will result in higher temperature and concentration values especially for the lower part of the channel.

1. Introduction

Study of heat and mass transfer in a channel has been one of the most appealing cases due to its several engineering applications in last decades [1–4]. In recent years, squeezing flow is one of the most interesting topics in the Computational Fluid Dynamic (CFD) studies. There are wide ranges of applications in which solid boundaries compress to squeeze out fluids in both technological and engineering processes. At the outset, the study will help to understand arterial blood flow. Besides, it is useful for the study of lubricating fluids, dampening shocks and polymer processing [5–7]. According to the squeezing flow studies, Rashidi et al. have used homotopy analysis method (HAM) to investigate the impact of either sucked or injected fluid, which flows into the stretching-penetrable surface, on heat and mass transfer characteristics of a nanofluid [8]. The influence of unsteady boundary conditions on heat and mass transfer properties of rotating Eyring–Powell (E–P) fluid has been studied by Nadeem et al. using optimal homotopy analysis method [9]. Agbaje et al. have studied the flow of unsteady (E–P) nanofluid over a shrinking surface. They have investigated the effect of heat generation and thermal radiation on velocity, temperature, and concentration fields, using a multi-domain bivariate spectral quasilinearization method [10]. For investigating the effect of thermal radiation and Joule heating on the heat and mass transfer properties of the E–P fluids, Hayat et al. have used HAM for obtaining the

* Corresponding author.
E-mail address: seyedi@wayne.edu (S. Hadi Seyedi).

https://doi.org/10.1016/j.physa.2019.124109
0378-4371/

Nomenclature

a	Distance between two walls
l	Initial distance
α	Wall motion parameter
$B(x)$	Magnetic field
Γ, δ	E–P fluid parameters
S	Squeeze Number
R	Thermal radiation
Ha	Hartmann number
Pr	Prandtl number
Q	Heat generation/absorption
Sc	Schmidt number
γ	Chemical reaction parameter
C_f	Skin friction coefficient
Nu	Nusselt number
Sh	Sherwood number
q_w	Wall heat flux
J_w	Mass flux
Re	Reynolds number
τ_w	Wall shear stress
I_ϕ	Operational Matrix of Integral for scaling functions
I_ψ	Operational Matrix of Integral for wavelets
V_j^r	Space spanned by the scaling functions
P_r	Legendre Polynomial of Degree r
$L_k(x)$	Lagrange Interpolating Polynomial
τ_k	Roots of Legendre Polynomials
$\phi^k(x)$	Alpert's Multiscaling Functions
ω_k	Gauss–Legendre Quadrature Weights
W_j^r	Complementary Orthogonal Subspaces
$\psi_{j,b}^k$	Multiwavelets
$\mathcal{P}_J^r$	Orthonormal Projection Operator
$\mathcal{M}_J^r$	Multiscale Operator
T_J	Wavelet Transform Matrix

temperature, velocity, and concentration fields on a stretching surface [11]. Reddy et al. considered the effects of heat generation/absorption and thermal radiation as well as magnetohydrodynamic flow on heat and mass transfer properties of two particular nanofluid on a stretching surface [12]. Duan–Rach Approach (DRA) utilized to investigate joule heating, Brownian diffusion, and thermophoresis effects on heat and mass transfer characteristics of MHD nanofluid flow between two non-parallel surfaces [13]. An electrically-heated micro-tube research has been conducted analytically. The finding confirms the influence of wall thickness and wall materials on temperature distribution. The effect of Joule heating, mixed electro-osmotic, and pressure driven along with constant surface heat flux on heat transfer characteristics of microchannel have been investigated analytically by Horiuchi et al. [14]. Periyadurai et al. have studied numerically the impact of magnetic field on the natural convection of Micro-polar fluid which flows in a square cavity with uniform and nonuniform horizontal/vertical heated thin plate, placed at the center of the cavity. Increasing Rayleigh number for both horizontal and vertical positions of the plate leads to increase heat transfer rate. Also, the uniform heat flux results in enhancing heat transfer in vertical position compared to the horizontal position case [15]. By investigating the effect of magnetohydrodynamic on non-Newtonian nanofluid flow in a pipe for variable viscosities, Ellahi shows the dependence of velocity and temperature field on the viscosity index [16]. To assess the effect of different external magnetic fields on heat transfer characteristics of magnetic nanofluid (ferrofluid), Control Volume based Finite Element Method (CVFEM) was utilized in a semi-annulus lid. In addition, they took into account the effects of both Ferrohydrodynamic (FHD) and Magnetohydrodynamic (MHD). The results show that the magnetic number and the Hartmann number rise because of the impact of FHD and MHD, respectively [17]. CVFEM was also used to study the effect of magnetic field dependent (MFD) viscosity on free convection heat transfer characteristics of nanofluid. The findings indicate that increasing the Rayleigh number and volume fraction of nanoparticle lead to rising in the Nusselt number but increasing the viscosity parameter and Hartmann number decrease the Nusselt number [18]. Using the Differential Transformation Method (DTM) to study

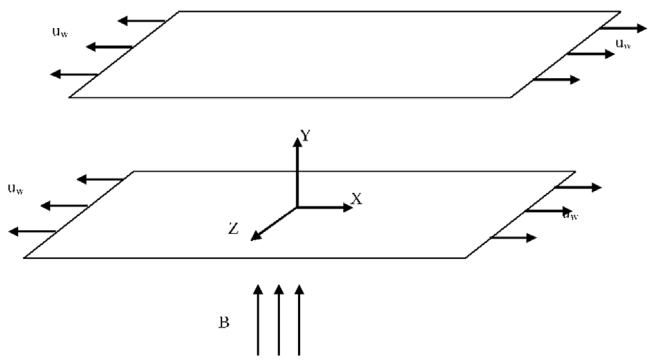

Fig. 1. The schematic of the problem, Eyring–Powell fluid between two walls.

the impact of the radiation parameter, squeezing number, Hartmann number and Brownian number on temperature, velocity, and concentration fields have been done in unsteady nanofluid flow between parallel plates. The results show that skin friction coefficient has correlated directly with Hartmann number and squeezing number [19]. Sheikholeslami et al. carried out research with the help of Control Volume based Finite Element Method (CVFEM) to study the changes of nanofluid heat transfer characteristics when nanofluid flow through a porous media. Consequently, thermal radiation leads to an increase in the average Nusselt number but rising Hartmann number results in Nusselt number decline [20]. Some useful contributions in this regard can be found in [21–30].

In reality, the study of non-Newtonian fluids is more complex and important than Newtonian fluids due to their critical and numerous applications such as toothpaste, ink, glues, food products and polymer solutions. Some mainly utilized models for the non-Newtonian fluids are power law, second grade, and Maxwell models. Nowadays, Eyring–Powell (E–P) model has been used a lot by the scholars in addition to the classical non-Newtonian models. The reason that this model is of great interest to engineers and scientist relies on different issues. One of the main advantages is, unlike the non-Newtonian models, its relations is not based on the empirical model, instead, kinetic theory of liquids has been used to derive the governing relations. In recent years developing nonlinear solvers has received more attention [31–33]. Using spectral and spectral element methods for solving linear differential equations in general and non-linear ones in particular, can provide higher accuracy in comparison to the other numerical methods [34,35]. Most of the researchers use common classical orthogonal polynomials as the basis in the Galerkin, Collocation or Tau methods in the spectral methods. We have used a relatively newly introduced Multi-wavelet basis and this combination provides some remarkable feature like multi-scale results and a higher rate of convergence. In our previous studies [35,36], we simulated the nanofluid squeezing flow in multi-scale format by a novel method. The results show that small changes in squeezing number can notably affect the temperature distribution. In the present study, a new Galerkin based method discussed and utilized to study the heat and mass transfer of an unsteady E–P squeezing flow by considering magnetic field, heat generation/absorption and Joule heating effects inside a stretching channel.

2. Problem description

Fig. 1 shows the schematic of the two-dimensional flow inside a squeezing channel in the presence of the magnetic field. Incompressible E–P fluid considered as the working fluid for this system. Also, the two horizontal walls of the channel are assumed to be infinite in length and are stretching with $U_w(x) = ax$. The distance between the two walls can be calculated based on $a(t) = \pm l(1 - \alpha t)^{0.5}$. In the mentioned formula, l is the initial distance of the walls and α gives motion to the walls based on time. Mathematically, $\alpha > 0$ means that the two walls are moving toward each other and helps the fluid to be squeezed. On the other hand, $\alpha < 0$ means that the two walls are moving away from each other. Effects of the magnetic field on the flow has shown by $B(x) = B_0(1 - \alpha t)^{-0.5}$. It should be mentioned that the effects of having thermal radiation, heat generation (or absorption), Lorentz force and Joule heating are considered in this study. The 2-D governing equations of the described problem can be written by use of the momentum, mass transfer, and energy equations in the unsteady format, as follows:

$$\frac{\partial u}{\partial x} + \frac{\partial v}{\partial y} = 0, \tag{1}$$

$$\frac{\partial u}{\partial t} + u\frac{\partial u}{\partial x} + v\frac{\partial u}{\partial y} = -\frac{1}{\rho}\frac{\partial P}{\partial x} + (\nu + \frac{1}{\rho\beta c})(\frac{\partial^2 u}{\partial x^2} + \frac{\partial^2 u}{\partial y^2}) - \frac{1}{3\rho\beta c^3}\frac{\partial}{\partial x}\left[\left(2(\frac{\partial u}{\partial x})^2 + 2(\frac{\partial v}{\partial y})^2 + (\frac{\partial u}{\partial y} + \frac{\partial v}{\partial x})^2\right)\frac{\partial u}{\partial x}\right]$$

$$- \frac{1}{6\rho\beta c^3}\frac{\partial}{\partial y}\left[\left(2(\frac{\partial u}{\partial x})^2+2(\frac{\partial v}{\partial y})^2+(\frac{\partial u}{\partial y}+\frac{\partial v}{\partial x})^2\right)(\frac{\partial u}{\partial y}+\frac{\partial v}{\partial x})\right]-\frac{\sigma B_0^2}{\rho(1-\alpha t)}u, \tag{2}$$

$$\begin{aligned}\frac{\partial v}{\partial t}+u\frac{\partial v}{\partial x}+v\frac{\partial v}{\partial y}&=-\frac{1}{\rho}\frac{\partial P}{\partial y}+(\nu+\frac{1}{\rho\beta c})(\frac{\partial^2 v}{\partial x^2}+\frac{\partial^2 v}{\partial y^2})\\&-\frac{1}{3\rho\beta c^3}\frac{\partial}{\partial y}\left[\left(2(\frac{\partial u}{\partial x})^2+2(\frac{\partial v}{\partial y})^2+(\frac{\partial u}{\partial y}+\frac{\partial v}{\partial x})^2\right)\frac{\partial v}{\partial y}\right]\\&-\frac{1}{6\rho\beta c^3}\frac{\partial}{\partial x}\left[\left(2(\frac{\partial u}{\partial x})^2+2(\frac{\partial v}{\partial y})^2+(\frac{\partial u}{\partial y}+\frac{\partial v}{\partial x})^2\right)(\frac{\partial u}{\partial y}+\frac{\partial v}{\partial x})\right],\end{aligned} \tag{3}$$

$$\frac{\partial T}{\partial t}+u\frac{\partial T}{\partial x}+v\frac{\partial T}{\partial y}=\frac{\kappa}{\rho C_P}(\frac{\partial^2 T}{\partial x^2}+\frac{\partial^2 T}{\partial y^2})+\frac{16\sigma^* T_0^3}{3\rho C_P k^*}\frac{\partial^2 T}{\partial y^2}+\frac{Q^*}{\rho C_P}(T-T_0)+\frac{\sigma B^2(x)}{\rho C_P}u^2, \tag{4}$$

$$\frac{\partial C}{\partial t}+u\frac{\partial C}{\partial x}+v\frac{\partial C}{\partial y}=D_m(\frac{\partial^2 C}{\partial x^2}+\frac{\partial^2 C}{\partial y^2})-\frac{k_1}{1-\alpha t}(C-C_0), \tag{5}$$

subject to the following boundary conditions:

$$\begin{aligned}&u=0,\quad v=v_w=\frac{da(t)}{dt},\quad T=T_0,\quad C=C_0\quad at\quad y=a(t)\\&v=\frac{\partial u}{\partial y}=\frac{\partial T}{\partial y}=\frac{\partial C}{\partial y}=0\quad at\quad y=0.\end{aligned} \tag{6}$$

By introducing the following non-dimensional variables, we have:

$$\eta=\frac{y}{l(1-\alpha t)^{\frac{1}{2}}},\quad u=\frac{\alpha x}{2(1-\alpha t)}\frac{df(\eta)}{d\eta},\quad v=-\frac{\alpha l}{2(1-\alpha t)^{\frac{1}{2}}}f(\eta),\quad \theta=\frac{T-T_0}{T_1-T_0},\quad \phi=\frac{C-C_0}{C_1-C_0}. \tag{7}$$

By using the non-dimensional variables of Eq. (7), Eq. (1) is the same as its initial equation, but Eqs. (2) and (3) lead to the following equation after eliminating the generalized pressure gradient.

$$(1+\Gamma)f^{iv}-S[\eta f'''+3f''+f'f''-ff''']-\Gamma\delta[2f''(f''')^2+(f'')^2f^{iv}]-Ha^2f''=0 \tag{8}$$

By virtue of Eq(7), Eqs. (4) and (5) take the following form:

$$(1+\frac{4}{3}R)\theta''+PrS(f\theta'-\eta\theta'+Q\theta)=0, \tag{9}$$

$$\phi''+ScS(f\phi'-\eta\phi')-Sc\gamma\phi=0, \tag{10}$$

$$\begin{aligned}&f(0)=0,\quad f''(0)=0,\quad f'(1)=0,\quad f(1)=1,\\&\theta'(0)=0,\quad \theta(1)=1,\quad \phi'(0)=0,\quad \phi(1)=1.\end{aligned} \tag{11}$$

In which, $\Gamma=\frac{1}{\mu\beta c}$ and $\delta=\frac{\alpha^2x^2}{8c^2l^2(1-\alpha t)^3}$ are E–P fluid parameters, $S=\frac{\alpha l}{2\nu}$, $R=\frac{4\sigma^*T_0^3}{\kappa k^*}$ denotes the squeezing number and the thermal radiation parameter, respectively. $Ha=B_0l\sqrt{\frac{\sigma}{\mu}}$ indicates the Hartmann number, $Pr=\frac{\mu C_P}{\kappa}$ is the Prantle number, and $Q=\frac{2Q^\star(1-\alpha t)}{\alpha\rho C_P}$ is the heat generation/absorption parameter which $Q<0$ implies heat absorption, but $Q>0$ represents heat generation. Also $Sc=\frac{\nu}{D_m}$ and $\gamma=\frac{l^2K_1}{\nu}$ represent the Schmidt number and the chemical reaction parameter, respectively. It is worthwhile to mention that E–P fluid parameter δ, which is depended on x, varies locally throughout the flow motion. Also, squeezing number S represents the movement of plates, which $S>0$ indicates channel stretching and $S<0$ shows channel shrinking. $\gamma>0$ is considered as a destructive chemical reaction, while $\gamma<0$ is a general chemical reaction. In addition, other physical properties such as skin-friction coefficient C_f, local Nusselt number Nu, and Sherwood number Sh are represented below:

$$C_f=\frac{\tau_w}{\rho v_w^2};\quad \tau_w=\left\{(\mu+\frac{1}{\beta c})\frac{\partial u}{\partial y}-\frac{1}{6\beta c^3}\left(\frac{\partial u}{\partial y}\right)^3\right\}|_{y=a(t)}\quad , \tag{12}$$

$$NU=\frac{lq_w}{\kappa(T_1-T_0)};\quad q_w=\left\{-\kappa\frac{\partial T}{\partial y}-\frac{16\sigma^*T_0^3}{3k^*}\frac{\partial T}{\partial y}\right\}|_{y=a(t)}\quad , \tag{13}$$

$$Sh=\frac{lJ_w}{D_m(C_1-C_0)};\quad J_w=D_m\frac{\partial C}{\partial y}|_{y=a(t)}. \tag{14}$$

In the above formulas, τ_w is the wall shear stress, q_w is the wall heat flux and J_w is the mass flux in the system. According to the non-dimensional variables in Eq. (7), one can write Eq. (12) for C_f, Eq. (13) for NU, and Eq. (14) for Sh like below:

$$Re_x \frac{l^2}{x^2} C_f = (1+\Gamma) f''(1) - \frac{\Gamma\delta}{3}[f''(1)]^3 \tag{15}$$

$$(1-\alpha t)^{\frac{1}{2}} NU = -(1+\frac{4}{3}R)\theta'(1), \quad (1-\alpha t)^{\frac{1}{2}} Sh = -\phi'(1), \tag{16}$$

where $Re_x = \frac{\alpha l x (1-\alpha t)^{\frac{1}{2}}}{2\nu}$ is the local squeeze Reynolds number.

3. Multi-wavelet Galerkin method (MWGM)

An orthogonal basis for $L^2(\mathbb{R})$ and $L^2([0,1])$ introduced by Alpert et al. [37,38] using multi-resolution analysis (MRA). In this system of wavelets, it is assumed that $\boldsymbol{\Phi}_J^r = \{\phi_{J,b}^k\}_{k=0,\ldots,r-1,b=0,\ldots,2^J-1}$ be an orthonormal basis for the Hilbert subspace $V_J^r \subset L^2[0,1)$ so that $\phi_{J,b}^k = 2^{\frac{J}{2}}\phi^k(2^J x - b)$ for $k = 0,\ldots,r-1$, $b = 0,\ldots,2^J-1$ can be made as follows. Also, assume that P_r is the Legendre polynomial of order r and $\{\tau_k\}_{k=0}^{r-1}$ denotes the roots of P_r. Suppose ω_k is the Gauss–Legendre quadrature weight.

$$\omega_k = \frac{2}{rP'_r(\tau_k)P_{r-1}(\tau_k)}.$$

By these assumptions, the interpolating scaling functions (*ISF*) are given in [36,39,40] and we have:

$$\phi^k(x) = \begin{cases} \sqrt{\frac{2}{\omega_k}} L_k(2x-1), & x \in [0,1], \\ 0, & \text{otherwise}, \end{cases}$$

where $L_k(x)$ is the Lagrange interpolating polynomial, defined by [41]

$$L_k(x) = \prod_{i=0, i\neq k}^{r-1} \frac{x-\tau_i}{\tau_k-\tau_i}, \quad k = 0,\ldots,r-1,$$

that they have characterized by Kronecker property $L_k(\tau_i) = \delta_{ik}$. Then we can define the projection $\mathcal{P}_J : L^2([0,1)) \to V_J^r$ via

$$f \approx \mathcal{P}_J(f)(x) = \sum_{k=0}^{r-1}\sum_{b=0}^{2^J-1} \langle f, \phi_{J,b}^k\rangle \phi_{J,b}^k(x) \approx \sum_{k=0}^{r-1}\sum_{b=0}^{2^J-1} f_{J,b}^k \phi_{J,b}^k(x). \tag{17}$$

where $f_{J,b}^k = 2^{-J/2}\sqrt{\frac{\omega_k}{2}} f\left(2^{-J}(\hat{\tau}_k + b)\right)$, $\hat{\tau}_k = \frac{\tau_k+1}{2}$, $k = 0,1,\ldots,r-1$, and $x \in [0,1)$ [42].

For each r, the system $\boldsymbol{\Phi}_J^r = \{\phi_{J,b}^k\}_{b=0,\ldots,2^J-1}$ defines a vector valued function $\Phi_J^r : [0,1) \to \mathbf{R}^n$ with $n = r2^J$ given, for all $x \in [0,1)$ by $\Phi_J^r := \left(\Phi_J^{r,0}, \Phi_J^{r,1}, \ldots, \Phi_J^{r,2^J-1}\right)^T$, where $\Phi_j^{r,b} = [\phi_{j,b}^0, \ldots, \phi_{j,b}^{r-1}]^T$. Therefore, one can write $\mathcal{P}_J(f)(x) = F^T\Phi_J^r(x)$, where F is a vector which consists of the coefficients $F_{br+k+1} := f_{J,b}^k$.

Alpert multi-wavelets satisfy in a matrix refinement equation

$$\Psi_0^{r,0} = \sum_{b=0}^{1} G^b D_2 T_b \Phi_0^{r,0}(x) = \sum_{b=0}^{1} G^b \Phi_1^{r,b}(x), \tag{18}$$

where $\Psi_j^{r,b} = D_{2^j} T_b \Psi_0^{r,0} = [\psi_{j,b}^0, \ldots, \psi_{j,b}^{r-1}]^T$, and $\{G^b\}$ are $(r \times r)$ matrices with constant elements. By this assumption there are $2r^2$ unknown coefficients in (18). We use the following $2r(r-1)$ vanishing moment conditions and $2r$ orthonormal conditions to determine them [36,43].

1. Vanishing moments: The moment of the Alpert multi-wavelets are defined as

$$\mathcal{N}_p^k = \int_{-\infty}^{\infty} x^p \psi^k(x)dx, \qquad p \geq 0, \text{ and } k = 0,1,\ldots,r-1.$$

The number of vanishing multi-wavelets moments for different k are denoted by $N_\psi^k = k + r - 1$,

$$\mathcal{N}_l^k = 0, \text{ for } 0 \leq l < N_\psi^k \text{ and } \mathcal{N}_{N_\psi^k}^k \neq 0,$$

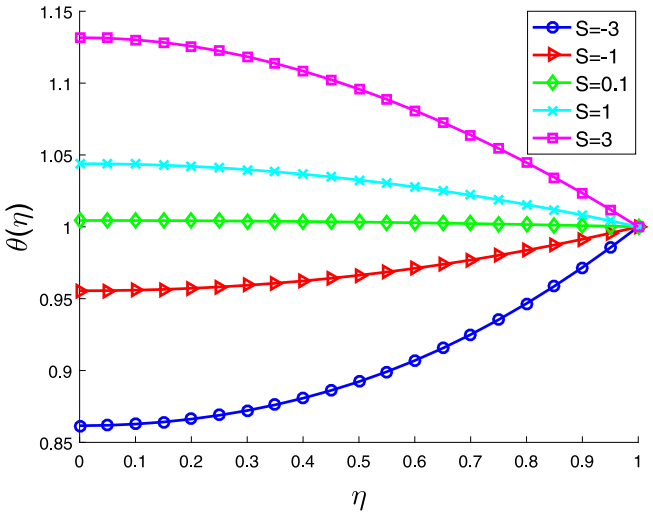

Fig. 2. The effect of squeezing parameter on the temperature profiles, when $\Gamma = S = Ha = Pr = \gamma = 1$, $Sc = R = Q = 0.1$ and $\delta = 0.01$.

2. Orthonormality:

$$\int_0^1 \psi^i(x)\psi^j(x)dx, \quad i, j = 0, 1, \ldots, r-1.$$

According to MRA properties, we have two kind of basis sets for $J \in \mathbf{N}$. One of them is vector valued function Φ_J^r (17) and the other is Ψ_J^r (vector function of multi-wavelets). Any function $f(x)$ on $L^2[0, 1)$ can be approximated using multi-wavelets as

$$\begin{aligned} f(x) \approx \mathcal{M}_J(f)(x) &= \sum_{k=0}^{r-1} \left\{ f_{0,0}^k \phi_{0,0}^k(x) + \sum_{j=0}^{J-1} \sum_{b=0}^{2^j-1} \tilde{f}_{j,b}^k \psi_{j,b}^k(x) \right\} \\ &= \tilde{F}^T \Psi_J^r(x), \end{aligned} \tag{19}$$

To find the components of matrix $\tilde{F}$, it is not necessary that these coefficients obtained by integration. To Avoid calculating these integrals, we use wavelet transform matrix T_J introduced which introduced previously in [36] via $\tilde{F}^T \approx F^T T_J^{-1}$.

We put all the pieces together and describe how to use the multi-wavelets Galerkin method for solving Eqs. (8)–(11). Suppose that $p_l^{(N)}$ for $l := 1, 2, 3$ is the largest derivative of p_l. Using Alpert's multi-wavelets, we can expand $p_l^{(N)}$ as

$$p_l^{(N)}(\eta) \approx \mathcal{M}_J^r(p_l^{(N)})(\eta) = P_l^T \Psi_J^r(\eta), \tag{20}$$

where P_l is the $(n \times 1)$ unknown vector. By "m" times integrating from both sides of Eq. (20), and using the operational matrix of integration I_ψ, introduced in [36,44], we get

$$p_l^{(N-m)}(\eta) \approx P_l^T I_\psi^m \Psi_J^r(\eta) + \sum_{i=1}^{m} p_l^{(N-i)}(0) \frac{x^{m-i}}{(m-i)!}, \tag{21}$$

where $p_l^{(N-i)}(0)$ for $i = 1, 2, \ldots, m$ is a known constant determined by boundary conditions or a unknown constant. However, we are able to expand $p_l^{(N-i)}(0)\frac{x^{m-i}}{(m-i)!}$ using Alpert's Multi-wavelets as

$$p_l^{(N-i)}(0)\frac{x^{m-i}}{(m-i)!} = \Lambda_{l,m,i}^T \Psi_J^r(\eta), \qquad i = 1, \ldots, m, \ \ l = 1, 2, 3. \tag{22}$$

Using (21) and (22), one has

$$p_l^{(N-m)}(\eta) \approx P_l^T I_\psi^m \Psi_J^r(\eta) + \sum_{i=1}^{m} \Lambda_{l,m,i}^T \Psi_J^r(\eta). \tag{23}$$

We are also able to expand the nonlinear terms of Eqs. (8)–(10) using multi-wavelets as

$$g_\iota(\eta) \approx \mathcal{M}_J^r(g_\iota)(\eta) = G_\iota^T \Psi_J^r(\eta), \quad \iota = 1, \ldots, 9, \tag{24}$$

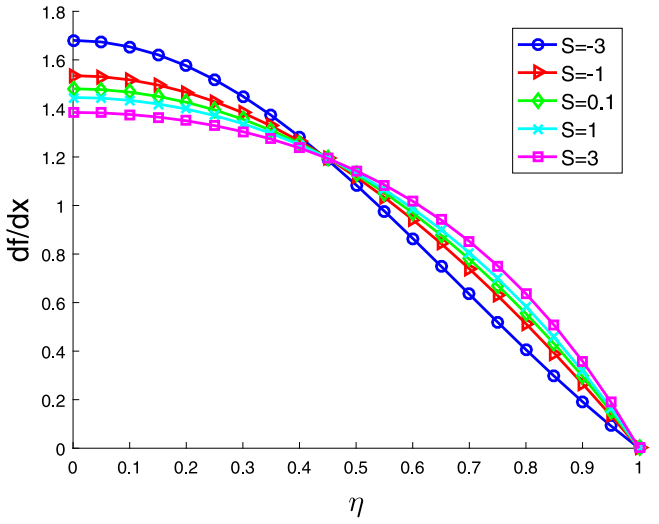

Fig. 3. The effect of squeezing parameters on velocity profiles, when $\Gamma = S = Ha = Pr = \gamma = 1$, $Sc = R = Q = 0.1$ and $\delta = 0.01$.

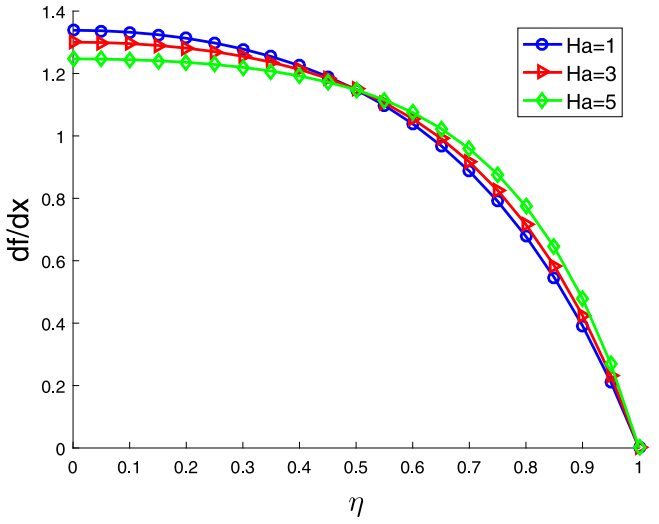

Fig. 4. The effect of Hartman numbers on velocity profiles when $\Gamma = S = Pr = \gamma = 1$, $Sc = R = Q = 0.1$ and $\delta = 0.01$.

where the entries of vectors G_ι are obtained by (17) and wavelet transform matrix, also

$$g_1 := \eta f'',\ g_2 := f' f'',\ g_3 := f f''',\ g_4 := f''(f''')^2,\ g_5 := (f'')^2 f^{iv},$$
$$g_6 := f\theta',\ g_7 := \eta\theta'\ g_8 := f\varphi',\ g_9 := \eta\varphi'.$$

Let us to look back into the Eqs. (8)–(10), using Eqs. (23), (24) and Multi-wavelet Galerkin method, we get

$$(1+\Gamma)P_1^T - S\left(G_1^T + (3+\frac{M^2}{S})(P_1^T I_\psi^2 + \sum_{i=1}^{2} \Lambda_{1,2,i}^T) + G_2^T - G_3^T\right) - \Gamma\delta\left(G_4^T + G_5^T\right) = 0,$$
$$(1+\frac{4}{3})P_2^T + PrS\left(G_6^T - G_7^T + Q(P_2^T I_\psi^2 + \sum_{i=1}^{2} \Lambda_{2,2,i}^T)\right) = 0,$$
$$P_3^T + ScS\left(G_8^T - G_9^T\right) - Sc\gamma(P_3^T I_\psi^2 + \sum_{i=1}^{2} \Lambda_{3,2,i}^T) = 0,$$

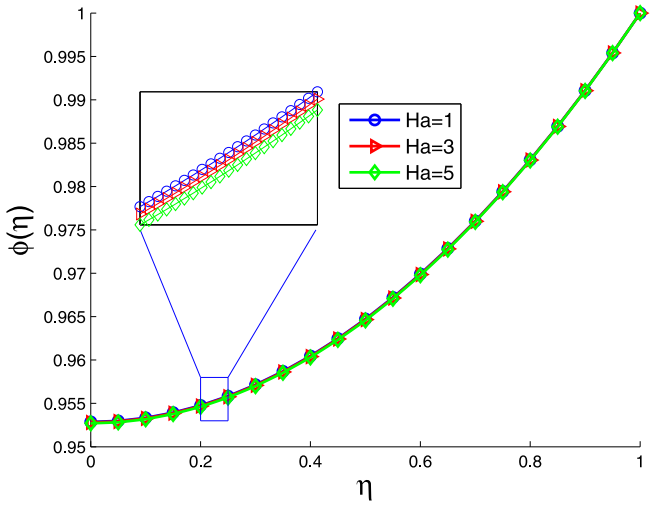

Fig. 5. The effect of Hartman numbers on the concentration profiles, when $S = 5$, $\Gamma = Pr = \gamma = 1$, $Q = R = Sc = 0.1$ and $\delta = 0.01$.

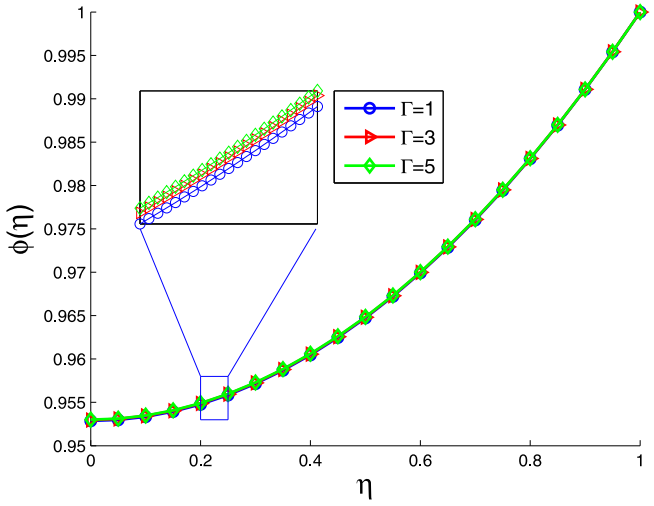

Fig. 6. The effect of fluid parameters on the concentration profiles, when $S = 5$, $Ha = Pr = \gamma = 1$, $Q = R = Sc = 0.1$ and $\delta = 0.01$.

where we assumed that $f = p_1$, $\theta = p_2$ and $\varphi := p_3$. These equations give a linear system of $3n - 4$ equations with $3n$ unknowns. Using the boundary conditions, we obtain four other equation. Therefore we can find the unknowns coefficients to find the solution of the system of Eqs. (8) to (10).

4. Results and discussion

In this section of the paper, we discuss the effects of the different input parameters on the solution of the governing equations and their physical interpretations on the temperature, velocity and concentration profiles. Before discussing the results of the simulation, we tested the written code and algorithm in different non-dimensional spacial values and for all f, θ and ϕ values for the validation and accuracy purposes. The obtained results compared to a valid Runge–Kutta method and as shown in Table 1, the results have excellent agreement with the Runge–Kutta method as a base method. Fig. 2 shows the effect of squeezing parameters S on the dimensionless temperature profiles. According to this figure, it is obvious that there is a direct relationship between the squeezing number and the temperature profile in the channel, which means that as the walls move apart from each other, the temperature will increase and the other way around. Fig. 2 also shows that we see various values for dimensionless temperatures when dimensionless variable η is zero; however, due to the Neumann boundary condition that we have at this point, we see zero slope for the temperature profiles. In addition, squeezing number $S = 0.1$ has almost no effect on temperature profile.

Table 1
Comparison of results for $f(\eta)$, $\theta(\eta)$, and $\phi(\eta)$ at various points when $S = 0.5$, $\delta = \Gamma = \gamma = 0.01$, $M = R = Pr = Q = 1$, and $Sc = 0.6$.

	Fourth order Runge–Kutta method [45]			Current method MWGM			Absolute errors		
η	$f(\eta)$	$\theta(\eta)$	$\phi(\eta)$	$f(\eta)$	$\theta(\eta)$	$\phi(\eta)$	e_f	e_θ	e_ϕ
0	0	1.11635116	0.97111743	0	1.11635116	0.97111743	0	0	0
0.1	0.14340981	1.11515547	0.97140872	0.14340981	1.11515547	0.97140872	0	0	0
0.2	0.28452102	1.11157316	0.97228200	0.28452102	1.11157316	0.97228200	0	0	0
0.3	0.42097009	1.10561826	0.97373563	0.42097009	1.10561826	0.97373563	0	0	0
0.4	0.55026183	1.09731328	0.97576714	0.55026183	1.09731328	0.97576714	0	0	0
0.5	0.66969914	1.08668785	0.97837367	0.66969898	1.08668785	0.97837367	1.61E−07	0	0
0.6	0.77630688	1.07377686	0.98155258	0.77630688	1.07377686	0.98155258	0	0	0
0.7	0.86674673	1.05861794	0.98530227	0.86674673	1.05861794	0.98530227	0	0	0
0.8	0.93721854	1.04124834	0.98962324	0.93721854	1.04124834	0.98962324	0	0	0
0.9	0.98334111	1.02170104	0.99451945	0.98334111	1.02170104	0.99451945	0	0	0
1	1	1	1	1	1	1	0	0	0

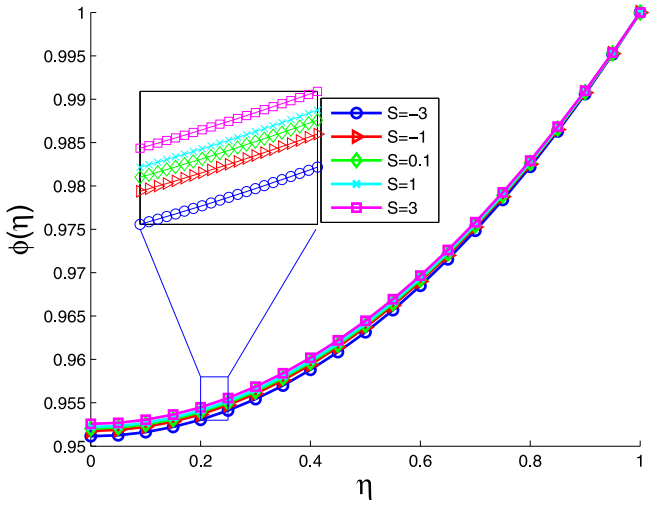

Fig. 7. The effect of squeezing parameters on the concentration profiles when $\Gamma = Ha = Pr = \gamma = 1$, $Sc = R = Q = 0.1$ and $\delta = 0.01$.

Figs. 3 and 4 represent the impact of variation of squeezing parameters and Hartman numbers on velocity profiles, respectively. The positive and negative squeezing numbers can affect the velocity profiles in two different ways. When $\eta < 0.45$, velocity profile will decrease by the decompression process (Fig. 3). However, there is a direct relationship between the velocity profile and the squeezing number after $\eta > 0.45$. Also, in Fig. 3, the velocity profile has maximum value for minimum squeezing number $S = -3$ and minimum value for maximum squeezing number $S = 3$ in the lower part of the channel. Similarly, according to Fig. 4, increasing the Hartman number decreases the velocity profile in the lower part of the channel, but this trend is reversed for velocity profile after dimensionless variable (η) reaches about 0.5.

Figs. 5 and 6 show the effect of variation of Hartman numbers and E–P fluid parameter Γ on the concentration profiles, respectively. For different Hartman numbers and Γ values, concentration profiles increase steadily based on the increase in non-dimensional distance parameter (η). Obtained results show that there is not a tangible change in concentration profiles for different Hartman and E–P fluid parameter, Γ. However, by having a close look at the results, one can observe that higher Hartman numbers, wind up having lower concentration values and higher Γ values result in higher concentration values along the channel.

The effect of a change in squeezing number on concentration profile is shown in Fig. 7. Concentration profile increases for various squeezing numbers with increasing the non-dimensional distance parameter (η). Results of the simulation revealed that highest concentration values can be obtained in the decompression mode.

The effect of the radiation parameter on the temperature profiles has been depicted in Fig. 8. As it could be predicted, increasing the radiation parameter will cause a higher heat transfer rate and this means that temperature profiles will drop. Therefore, higher radiation parameters will cause lower temperature profile distributions.

The impact of E–P fluid parameter Γ and Hartman number on temperature profiles can be found in Figs. 9 and 10. According to Fig. 9, there is a reverse relationship between the E–P fluid parameter Γ and the temperature values all over the channel. It should be mentioned that the effects of the Γ on the temperature profile is more notable in the lower part of the channel. Fig. 10 illustrates the direct effect of the Hartman number on the temperature profiles. Higher Hartman

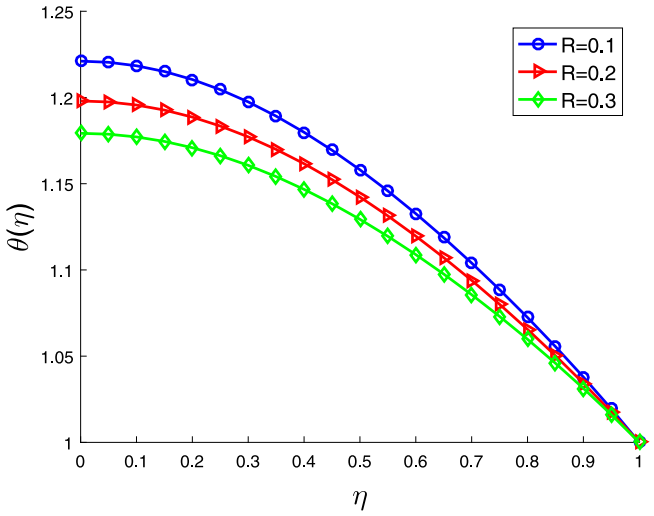

Fig. 8. The effect of radiation parameters on temperature profiles when S=5, $\Gamma = Ha = Pr = \gamma = 1$, $Sc = Q = 0.1$ and $\delta = 0.01$.

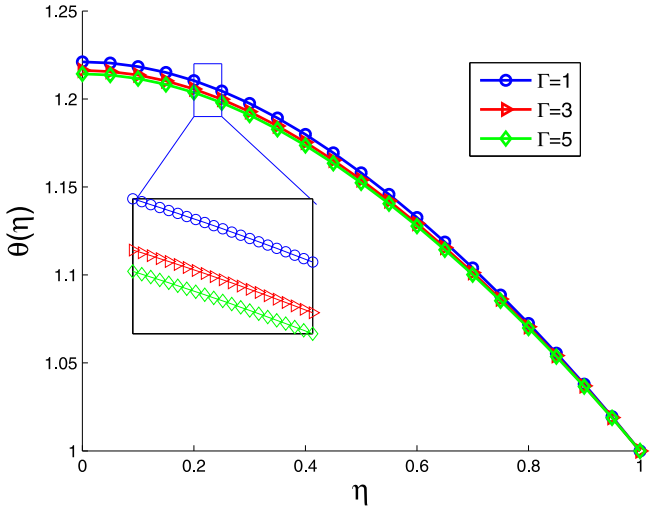

Fig. 9. The effect of fluid parameters on temperature profile when $S = 5$, $Ha = Pr = \gamma = 1$, $Sc = Q = R = 0.1$ and $\delta = 0.01$.

numbers decrease the heat transfer rate and cause the fluid flow to experience a higher temperature. Again, this effect is more remarkable in the lower part of the channel due to the special physics of the problem.

The graph in Fig. 11 shows the effect of heat generation/absorption parameters on the temperature profiles. When we have an exothermic chemical reaction $Q > 0$, increase in the heat generation parameter will elevate the temperature distribution. For the heat absorption cases $Q < 0$, higher absorption rate in the chemical reaction will soak up the heat more and the temperature profile will drop inside the channel (see Fig. 11).

Fig. 12 depicts the Schmidt number on the concentration profiles. One can see that higher Schmidt number corresponds to lower concentration values along the channel. Based on the definition of the Schmidt number, which defines the ratio of momentum diffusivity and mass diffusivity, lower Schmidt numbers correspond to higher mass diffusivity and higher mass diffusion will cause higher concentration for the (E–P) fluid.

5. Conclusion

The two-dimensional flow of a non-Newtonian Eyring–Powell fluid which squeezed between infinite flat plates considered. The governing equations for the momentum, heat and mass transfer, transformed by non-dimensional variables to a set of non-linear coupled differential equations. The resulted equations solved by a high accuracy numerical method based on the Galerkin method with Multi-wavelet basis (MWGM). The obtained numerical results are compared with the existing numerical solutions in the literature and high accuracy of the current method is demonstrated. Moreover,

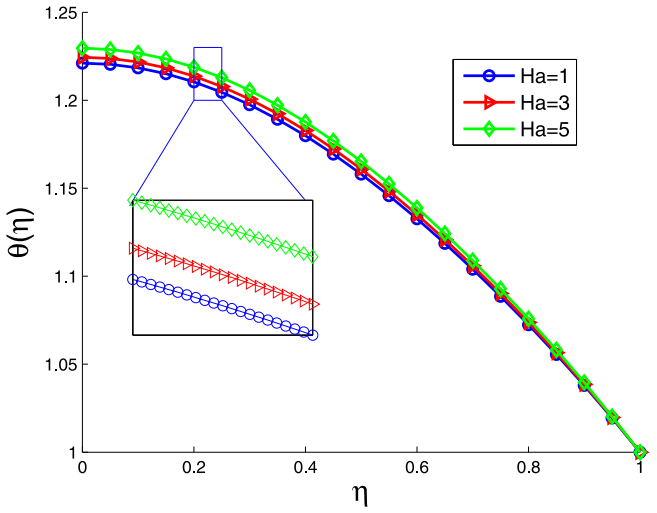

Fig. 10. The effect of Hartman numbers on temperature profile when $S = 5$, $\Gamma = Pr = \gamma = 1$, $Sc = Q = R = 0.1$ and $\delta = 0.01$.

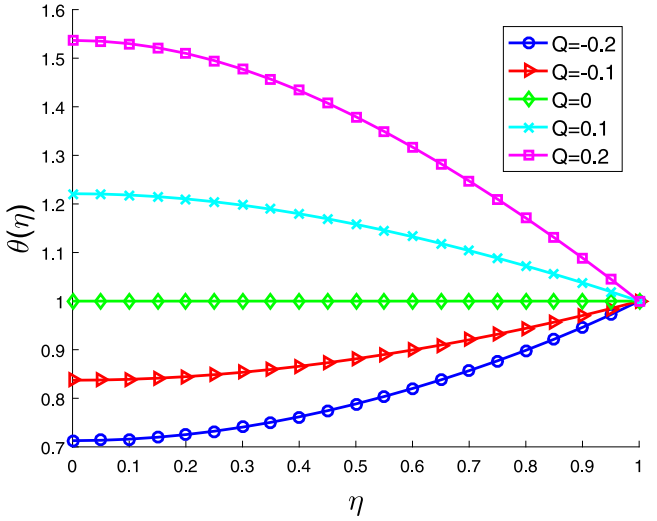

Fig. 11. The effect of heat generation/absorption parameters on the temperature profiles when $S = 5$, $\Gamma = Ha = Pr = \gamma = 1$, $Sc = R = 0.1$ and $\delta = 0.01$.

the effects of different situations and conditions were taken into account including heat radiation, magnetic forces, heat generation/absorption, and Joule heating effects. The results showed that the velocity profile shows a dual behavior for the change in the Hartman and squeezing numbers. Also, It revealed that by increasing the E–P fluid parameter Γ the temperature profile will drop; however, the concentration of the fluid will increase. The proposed method can be utilized for the multi-scale simulation of the complex and highly non-linear problems in science and engineering.

Declaration of competing interest

The authors declare that they have no known competing financial interests or personal relationships that could have appeared to influence the work reported in this paper.

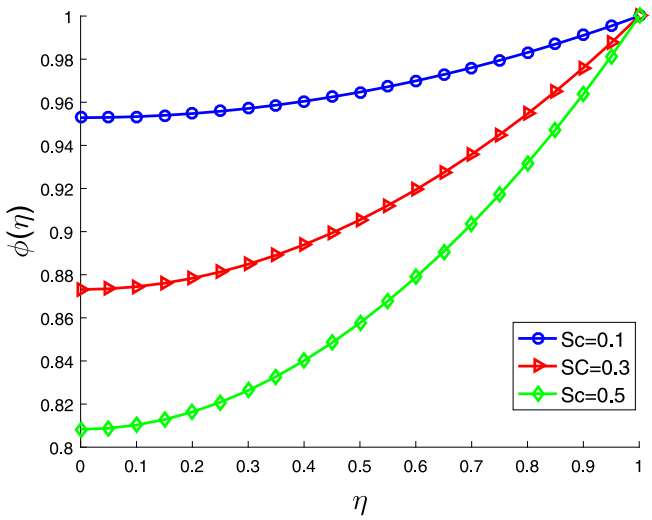

Fig. 12. The effect of Schmidt numbers on the concentration profiles when $S = 5$, $\Gamma = Ha = Pr = \gamma = 1$, $Q = R = 0.1$ and $\delta = 0.01$.

References

[1] R.W. Bruce, T.Y. Na, Natural Convection Flow of Powell-Eyring Fluids Between Two Vertical Flat Plates, ASME, 1967.
[2] Kumbakonam R. Rajagopal, Tsung-Yen Na, Natural convection flow of a non-Newtonian fluid between two vertical flat plates, Acta Mech. 54 (3–4) (1985) 239–246.
[3] Z. Ziabakhsh, G. Domairry, Analytic solution of natural convection flow of a non-Newtonian fluid between two vertical flat plates using homotopy analysis method, Commun. Nonlinear Sci. Numer. Simul. 14 (5) (2009) 1868–1880.
[4] S.H. Seyedi, Behzad Nemati Saray, M.R.H. Nobari, Using interpolation scaling functions based on Galerkin method for solving non-Newtonian fluid flow between two vertical flat plates, Appl. Math. Comput. 269 (2015) 488–496.
[5] Jan Engmann, Colin Servais, Adam S. Burbidge, Squeeze flow theory and applications to rheometry: a review, J. Non-Newton. Fluid Mech. 132 (1–3) (2005) 1–27.
[6] W.L. Lim, Y.T. Chew, H.T. Low, W.L. Foo, Cavitation phenomena in mechanical heart valves: the role of squeeze flow velocity and contact area on cavitation initiation between two impinging rods, J. Biomech. 36 (9) (2003) 1269–1280.
[7] C. Shah Rajesh, M.V. Bhat, Ferrofluid squeeze film in a long journal bearing, Tribol. Int. 37 (6) (2004) 441–446.
[8] M.M. Rashidi, A. Freidoonimehr, O. Hosseini, N. Anwar Bég, T.-K. Hung, Homotopy simulation of nanofluid dynamics from a non-linearly stretching isothermal permeable sheet with transpiration, Meccanica 49 (2) (2014) 469–482.
[9] S. Nadeem, S. Saleem, Mixed convection flow of Eyring–Powell fluid along a rotating cone, Results Phys. 4 (2014) 54–62.
[10] T.M. Agbaje, S. Mondal, P. Sibanda, A numerical study of unsteady non-Newtonian Powell-Eyring nanofluid flow over a shrinking sheet with heat generation and thermal radiation, Alex. Eng. J. 56 (1) (2017) 81–91.
[11] T. Hayat, Sh Ali, A. Alsaedi, H.H. Alsulami, Influence of thermal radiation and Joule heating in the Eyring–Powell fluid flow with the Soret and Dufour effects, J. Appl. Mech. Tech. Phys. 57 (6) (2016) 1051–1060.
[12] P. Sudarsana Reddy, Ali J. Chamkha, Soret and Dufour effects on MHD convective flow of Al2O3–water and TiO2–water nanofluids past a stretching sheet in porous media with heat generation/absorption, Adv. Powder Technol. 27 (4) (2016) 1207–1218.
[13] A.S. Dogonchi, D.D. Ganji, Analytical solution and heat transfer of two-phase nanofluid flow between non-parallel walls considering joule heating effect, Powder Technol. 318 (2017) 390–400.
[14] Keisuke Horiuchi, Prashanta Dutta, Akram Hossain, Joule-heating effects in mixed electroosmotic and pressure-driven microflows under constant wall heat flux, J. Eng. Math. 54 (2) (2006) 159.
[15] K. Periyadurai, M. Muthtamilselvan, Deog-Hee Doh, Influence of inclined Lorentz force on micropolar fluids in a square cavity with uniform and nonuniform heated thin plate, J. Magn. Magn. Mater. 420 (2016) 343–355.
[16] R. Ellahi, The effects of MHD and temperature dependent viscosity on the flow of non-newtonian nanofluid in a pipe: analytical solutions, Appl. Math. Model. 37 (3) (2013) 1451–1467.
[17] Mohsen Sheikholeslami, Kuppalapalle Vajravelu, Mohammad Mehdi Rashidi, Forced convection heat transfer in a semi annulus under the influence of a variable magnetic field, Int. J. Heat Mass Transfer 92 (2016) 339–348.
[18] M. Sheikholeslami, M.M. Rashidi, T. Hayat, D.D. Ganji, Free convection of magnetic nanofluid considering MFD viscosity effect, J. Molecular Liquids 218 (2016) 393–399.
[19] M. Sheikholeslami, D.D. Ganji, M.M. Rashidi, Magnetic field effect on unsteady nanofluid flow and heat transfer using Buongiorno model, J. Magn. Magn. Mater. 416 (2016) 164–173.
[20] M. Sheikholeslami, S.A. Shehzad, CVFEM simulation for nanofluid migration in a porous medium using Darcy model, Int. J. Heat Mass Transfer 122 (2018) 1264–1271.
[21] Navid Balazadeh, M. Sheikholeslami, Davood Domairry Ganji, Zhixiong Li, Semi analytical analysis for transient Eyring-Powell squeezing flow in a stretching channel due to magnetic field using DTM, J. Molecular Liquids 260 (2018) 30–36.
[22] Hafiz Muhammad Ali, Hassan Ali, Hassan Liaquat, Hafiz Talha Bin Maqsood, Malik Ahmed Nadir, Experimental investigation of convective heat transfer augmentation for car radiator using ZnO–water nanofluids, Energy 84 (2015) 317–324.
[23] Hafiz Muhammad Ali, Muhammad Danish Azhar, Musab Saleem, Qazi Samie Saeed, Ahmed Saieed, Heat transfer enhancement of car radiator using aqua based magnesium oxide nanofluids, Therm. Sci. 19 (6) (2015).
[24] S.S. Ghadikolaei, Kh. Hosseinzadeh, D.D. Ganji, Analysis of unsteady MHD Eyring-Powell squeezing flow in stretching channel with considering thermal radiation and Joule heating effect using AGM, Case Stud. Therm. Eng. 10 (2017) 579–594.

[25] Hafiz Muhammad Ali, Waqas Arshad, Thermal performance investigation of staggered and inline pin fin heat sinks using water based rutile and anatase TiO2 nanofluids, Energy Convers. Manag. 106 (2015) 793–803.
[26] Hafiz Muhammad Ali, Waqas Arshad, Effect of channel angle of pin-fin heat sink on heat transfer performance using water based graphene nanoplatelets nanofluids, Int. J. Heat Mass Transfer 106 (2017) 465–472.
[27] M. Mustafa, T. Hayat, S. Obaidat, On heat and mass transfer in the unsteady squeezing flow between parallel plates, Meccanica 47 (7) (2012) 1581–1589.
[28] Arshad. Waqas, Hafiz Muhammad Ali, Graphene nanoplatelets nanofluids thermal and hydrodynamic performance on integral fin heat sink, Int. J. Heat Mass Transfer 107 (2017) 995–1001.
[29] Muhammad Usman Sajid, Hafiz Muhammad Ali, Thermal conductivity of hybrid nanofluids: a critical review, Int. J. Heat Mass Transfer 126 (2018) 211–234.
[30] Muhammad Usman Sajid, Hafiz Muhammad Ali, Recent advances in application of nanofluids in heat transfer devices: a critical review, Renew. Sustain. Energy Rev. 103 (2019) 556–592.
[31] Hao-Nan Xu, Wei-Yong Ruan, Xing Lü, Multi-exponential wave solutions to two extended Jimbo–Miwa equations and the resonance behavior, Appl. Math. Lett. 99 (2020) 105976.
[32] Yan-Fei Hua, Bo-Ling Guo, Wen-Xiu Ma, Xing Lü, Interaction behavior associated with a generalized (2+ 1)-dimensional Hirota bilinear equation for nonlinear waves, Appl. Math. Model. 74 (2019) 184–198.
[33] Yu-Hang Yin, Wen-Xiu Ma, Jian-Guo Liu, Xing Lü, Diversity of exact solutions to a (3+ 1)-dimensional nonlinear evolution equation and its reduction, Comput. Math. Appl. 76 (6) (2018) 1275–1283.
[34] Seyedhadi Seyedi, Multiresolution solution of Burgers equation with B-spline wavelet basis, 2018, arXiv preprint arXiv:1812.10117.
[35] S. Hadi Seyedi, Behzad Nemati Saray, Ali Ramazani, High-accuracy multiscale simulation of three-dimensional squeezing carbon nanotube-based flow inside a rotating stretching channel, Math. Probl. Eng. 2019 (2019).
[36] S. Hadi Seyedi, Behzad Nemati Saray, Ali Ramazani, On the multiscale simulation of squeezing nanofluid flow by a highprecision scheme, Powder Technol. 340 (2018) 264–273.
[37] Beylkin Alpert, Gregory Beylkin, David Gines, Lev Vozovoi, Adaptive solution of partial differential equations in multiwavelet bases, J. Comput. Phys. 182 (1) (2002) 149–190.
[38] Bradley Alpert, Gregory Beylkin, Ronald Coifman, Vladimir Rokhlin, Wavelet-like bases for the fast solution of second-kind integral equations, SIAM J. Sci. Comput. 14 (1) (1993) 159–184.
[39] M. Shamsi, M. Razzaghi, Numerical solution of the controlled duffing oscillator by the interpolating scaling functions, J. Electromagn. Waves Appl. 18 (5) (2004) 691–705.
[40] Behzad Nemati Saray, Mehrdad Lakestani, Mohsen Razzaghi, Sparse representation of system of Fredholm integro-differential equations by using alpert multiwavelets, Comput. Math. Math. Phys. 55 (9) (2015) 1468–1483.
[41] Mostafa Shamsi, Mohsen Razzaghi, Solution of Hallen's integral equation using multiwavelets, Comput. Phys. Commun. 168 (3) (2005) 187–197.
[42] Behzad Nemati Saray, Mehrdad Lakestani, Carlo Cattani, Evaluation of mixed Crank–Nicolson scheme and Tau method for the solution of Klein–Gordon equation, Appl. Math. Comput. 331 (2018) 169–181.
[43] Nemati Saray Behzad, Jalil Manafian, Sparse representation of delay differential equation of Pantograph type using multi-wavelets Galerkin method, Eng. Comput. 35 (2) (2018) 887–903.
[44] Behzad Nemati Saray, An efficient algorithm for solving Volterra integro-differential equations based on Alpert's multi-wavelets Galerkin method, J. Comput. Appl. Math. 348 (2019) 453–465.
[45] Samuel Olumide Adesanya, Hammed Abiodun Ogunseye, Srinivas Jangili, Unsteady squeezing flow of a radiative Eyring-Powell fluid channel flow with chemical reactions, Int. J. Therm. Sci. 125 (2018) 440–447.